

# Diverse and Lifespan Facial Age Transformation Synthesis with Identity Variation Rationality Metric

Jiu-Cheng Xie, *member, IEEE*, Jun Yang, Wenqing Wang, Feng Xu, Hao Gao, *member, IEEE*

**Abstract**—Face aging has received continuous research attention over the past two decades. Although previous works on this topic have achieved impressive success, two longstanding problems remain unsettled: 1) generating diverse and plausible facial aging patterns at the target age stage; 2) measuring the rationality of identity variation between the original portrait and its syntheses with age progression or regression. In this paper, we introduce DLAT<sup>+</sup>, the first algorithm that can realize Diverse and Lifespan Age Transformation on human faces, where the diversity jointly manifests in the transformation of facial textures and shapes. Apart from the diversity mechanism embedded in the model, multiple consistency restrictions are leveraged to keep it away from counterfactual aging syntheses. Moreover, we propose a new metric to assess the rationality of Identity Deviation under Age Gaps (IDAG) between the input face and its series of age-transformed generations, which is based on statistical laws summarized from plenty of genuine face-aging data. Extensive experimental results demonstrate the uniqueness and effectiveness of our method in synthesizing diverse and perceptually reasonable faces across the whole lifetime.

**Index Terms**—Facial age transformation, diverse aging synthesis, geometric and textural manipulation, identity preservation, generative adversarial network.

## I. INTRODUCTION

WITH a human portrait, facial age transformation synthesis aims to simulate the corresponding appearance at the target age stage, which is user-specified. In the past two decades, this topic has attracted numerous attention in the computer vision community. The reasons for continuous concerns partially come from its relevant applications: special effects production in film animation entertainment and searching for people lost for many years. Advances in these fields will bring substantial economic and social benefits.

Most early efforts at facial age transformation study the transition between adults and the elderly, during which the facial changes are mainly at the texture level (e.g., the increase or decrease of the wrinkles, the changes in hair color and

amount). Benefiting from the rapid progress in generative networks (e.g., from StyleGAN1 to StyleGAN3 [1]–[3]) and the open access of face datasets (e.g., FFHQ [4]) characterized by comprehensive age coverage from infancy to senectitude along with a large number of high-resolution portraits under each certain period, LATS [5] comes out as the groundbreaking work in realizing lifelong age transformation synthesis. After that, several researchers proposed respective methods [6]–[10], pushing research in this field to new boundaries. While these algorithms achieve impressive performance, they share a common limitation with previous works: **the generated faces of the given subject under the target age condition look the same**. In other words, these models can just simulate deterministic age regression or progression effects, which is contrary to the universal facial aging rules in reality. In short, human growth is affected not only by internal factors dependent on age-related genes but also by many external factors, including lifestyle, climate, professions, etc. Uncertainty in these aspects determines that there should be infinite candidates for a subject’s possible appearance at the specified age stage. Liu et al. [11] made the first and only attempt to address the diverse aging problem. Apart from the input portrait for the age transformation purpose, their technique needs another facial image to provide age-relevant information, which is the origin of diverse signals. However, the design based on a real reference face also hinders their wide applications in practice.

Most of the time, we do not have the input subject’s portrait at the target age phases in the real world, so it is difficult to accurately evaluate the reasonability of identity variation between the source and synthesized faces. To achieve quantitative evaluation, some works [9], [12]–[14] taken an alternative scheme through conducting verification tests between input and generated faces, while the similarity score above a predefined threshold will be regarded as a successful verification and the opposite as a failed case. Regarding performance evaluation, **they simply equate the higher verification rate with more reasonable identity preservation between original and age-transformed face pairs**. We argue that this equivalence does not hold. In alignment with our opinion, [15] also reported the following observation according to their experiments: “as the time interval of age progression increases, both confidence scores and verification rates gradually decrease”.

To deal with the issues mentioned above, in this paper, we present DLAT<sup>+</sup>, the first method for Diverse and Lifespan Age Transformation on facial images according to our knowledge. The full model is composed of two sub-

This work was supported in part by National Nature Science Foundation of China under Grant 62301278, Grant 62371254, Grant 61931012; in part by Nature Science Foundation of Jiangsu Province of China under Grant BK20230362 and Grant BK20210594; and in part by Natural Science Research Start-up Foundation of Recruiting Talents of Nanjing University of Posts and Telecommunications under Grant NY222019 and Grant NY221019. (Corresponding author: Hao Gao.)

Jiu-Cheng Xie, Jun Yang and Hao Gao are with the College of Automation and College of Artificial Intelligence, Nanjing University of Posts and Telecommunications, Nanjing 210003, China (e-mail: jiu-chengxie@gmail.com; perryj200009@gmail.com; tsgaohao@gmail.com).

Wenqing Wang is with the Centre for Vision, Speech and Signal Processing (CVSSP), University of Surrey, GU2 7XH Guildford, U.K. (e-mail: wenqing.wang@surrey.ac.uk).

Feng Xu is with the School of Software and BNRist, Tsinghua University, Beijing 100190, China (email: xufeng2003@gmail.com).

networks, namely  $DLAT_{img}$  and  $DLAT_{lmk}$ . The former is able to realize photorealistic simulation of the given subject at desired age stages across the whole life cycle, but with diverse aging patterns mainly manifesting at the texture level. The latter is used to compensate for the shortage of facial shape diversity, while this rectification is achieved through leveraging the transformation parameters yielded by  $DLAT_{lmk}$  to warp the output face obtained from  $DLAT_{img}$ . A shared principle of diversity mechanism is embedded in these two networks during their respective model's training processes. In short, this mechanism first constructs the mapping from noise to age latent codes associated with specific age stages. Then, it forces the generator to synthesize faces located in expected age phases via conditioning on corresponding age codes. After this procedure, the connection between noise and multiple age-related latent distributions has been established. Then, various aging effects can be achieved through random noise sampling. Noting that we devise a series of constraints based on identity, race, and pose consistency between corresponding face pairs before and after age transition to protect the model from excessive and unreasonable facial aging diversity. In addition, we analyze the variations of identity similarity among portraits at different age stages from the same subjects, who are contained in two public real face datasets with accurate age labels. As a result, we obtain the general laws of identity similarity changes across ages in reality. Based on this rule, we design a metric called **Identity Deviation under Age Gaps (IDAG)**, which assesses identity variation rationality during facial age transformation.

To summarize, the contributions of this paper are as follows:

- A new method for synthesizing diverse and plausible facial aging effects, where the target age stages cover the whole life cycle. Concretely, the proposed diversity mechanism is separately deployed to the generations of facial texture and shape, and then respective synthetic intermediates are fused through image warping. Besides, consistency restrictions of race, pose, and identity are applied to the model, making aging diversity within an appropriate range.
- A new metric for measuring the identity variation rationality between source faces and corresponding age-transformed generations, which essentially compares the identity change trends synthesized with universal variation rules in the real world.
- Extensive experiments demonstrate our method's unique ability to realize diverse age transformations compared to the latest techniques. In addition, under more challenging settings where gaps between source and target age stages are decades, our approach shows better identity shift reasonability and lower age transition errors than others.

## II. RELATED WORK

### A. Facial Age Transformation

Early efforts at facial age transformation predominantly relied on traditional computer vision methods. These approaches often employ techniques such as geometric morphing [16]–[18], texture synthesis [19]–[21], and statistical models to

simulate age progression or regression [22]–[25]. However, these methods were limited in capturing intricate facial details and often produced unrealistic results. The advent of deep generative models (DGMs) marked a significant paradigm shift in facial age transformation research. Notable contributions include the works of Zhang et al. [26] and Antipov et al. [27], where conditional adversarial autoencoder and conditional generative adversarial networks (cGANs) were employed respectively to generate facial images conditioned on age labels. These two pioneering works demonstrated the capacity of DGMs to produce high-quality, age-transformed faces with improved realism. Subsequent researchers have explored various modifications and extensions of conditional generative architectures to enhance their performance in facial age transformation tasks [15], [28]–[32]. Recent research cares about more challenging yet practical settings, such as 3D face aging [33], high-resolution aging results [34]–[36], lifelong aging synthesis [5]–[9], background structure [10] and personality preservation [12], [37]. Compared to previous literature, our work extends the direction explored by [5]–[9] and [11] to a more practical yet challenging setting, that is, realizing diverse age transformation across the whole lifecycle. Note that this scenario is closer to human aging processes in reality.

### B. Controllable Face Editing

Face aging is closely connected to controllable face editing, which aims to alter specific attributes of a facial image (such as gender, hairstyle, expression, etc.) while keeping others unchanged. This task has been extensively studied in the past few years [38]–[50]. For a more detailed survey in this field, please refer to [51]. According to their different operating modes, we roughly classify those approaches into two categories: training models from scratch with given control conditions [38]–[42] or manipulating relevant latent representations in a pre-trained GAN's feature space [43]–[50]. Under this taxonomy, our method belongs to the former. Although approaches of the latter escape from heavy training burdens, they need to afford the costs of rough attribute editing. For example, there are only binary choices in their application to facial age transformation: younger or older, whereas specialist algorithms can achieve more fine-grained manipulation up to specific age stages.

## III. METHOD

Given a facial photo of one person, our basic Diverse and Lifespan Age Transformation ( $DLAT_{img}$ ) model is able to synthesize *diverse age progression or regression effects across the whole life cycle* on the subject's face. In addition, we introduce its counterpart based on facial landmarks ( $DLAT_{lmk}$ ) to focus on learning facial geometry deformation during the aging process. Collaborations between them through image-warping lead to a more powerful version dubbed  $DLAT^+$ , which can yield age-transformed faces with more variety and reasonability in terms of facial texture and shape.

### A. Diverse and Lifespan Age Transformation

Denoting the given facial image as  $X$ , our  $DLAT_{img}$  model takes it and random noise  $n$  as joint inputs and then produces

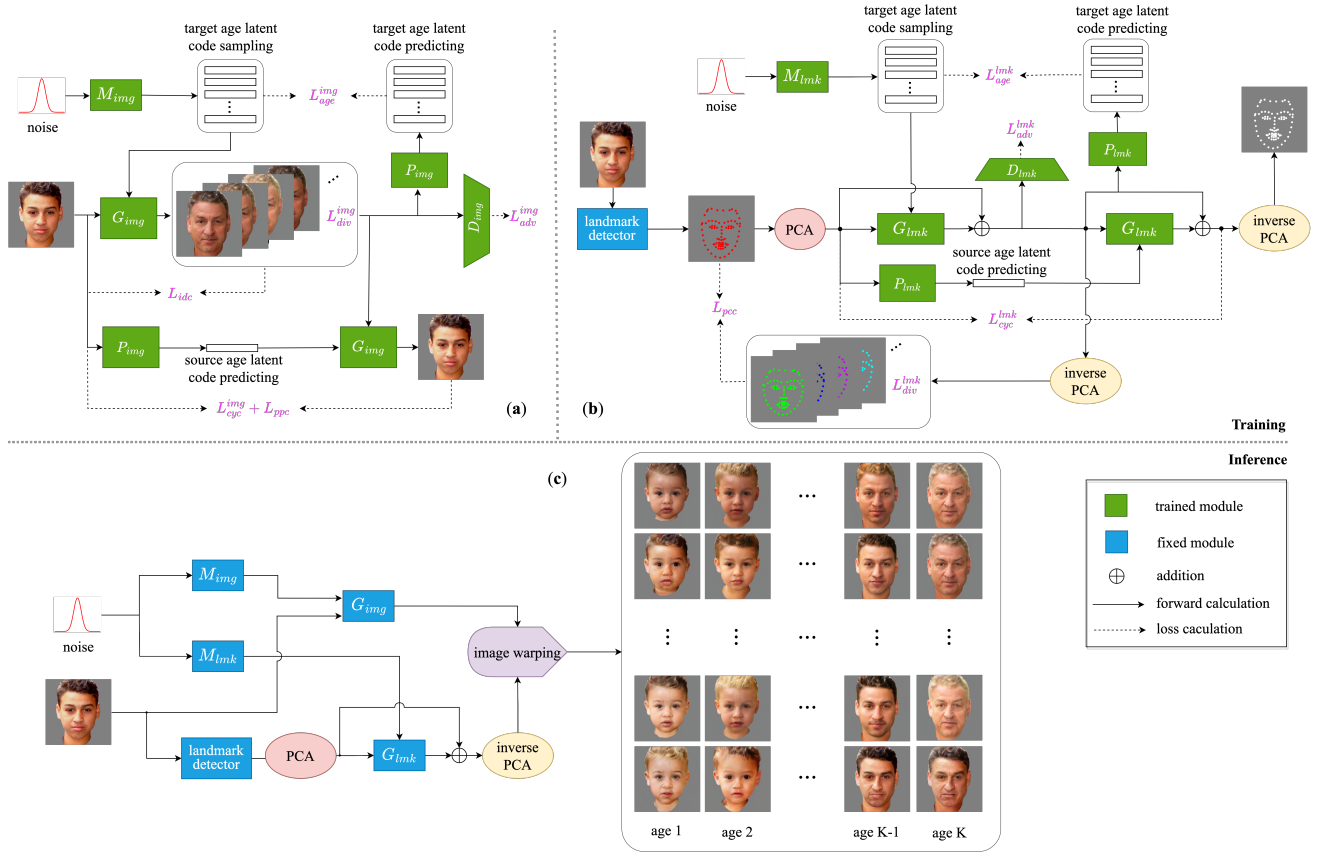


Fig. 1. An overview of our method. During the training stage, the proposed  $DLAT_{img}$  (a) and  $DLAT_{lmck}$  (b) are learned separately. After that procedure, relevant generators and mapping modules used to obtain age-latent codes are picked out with fixed parameters from the above two networks. They further constitute the  $DLAT^+$  (c), which is able to simulate diverse and lifelong age transformation effects on the given input faces.

a sequence of synthesized corresponding faces under user-predefined age stages  $\{\mathbf{Y}_k\}_{k=1}^K$ . Note that adjusting the input noise will lead to distinct but reasonable aging effects. This is formulated as

$$\{\mathbf{Y}_k\}_{k=1}^K = DLAT_{img}(\mathbf{X}, \mathbf{n}), \quad \mathbf{n} \sim \mathcal{N}(\boldsymbol{\mu}, \boldsymbol{\Sigma}) \quad (1)$$

where  $\boldsymbol{\mu}$  and  $\boldsymbol{\Sigma}$  denote the mean and covariance matrix of the multivariate normal distribution chosen, and  $K$  is the total number of different age phases considered. The training of  $DLAT_{img}$  involves four separate network modules, namely diverse age mapping network  $M_{img}$ , face generator  $G_{img}$ , age latent code predictor  $P_{img}$  and the image discriminator  $D_{img}$ . While in the inference stage, only the former two components are used. Fig. 1(a) depicts the framework of the proposed  $DLAT_{img}$ .

**Diverse age mapping module.** Our diverse age mapping module converts a piece of noise into a set of age latent codes,  $\{\mathbf{u}_k\}_{k=1}^K = M_{img}(\mathbf{n})$ , corresponding to non-overlapped and ordinal age stages. Through random noise sampling, this module is expected to produce various but correlated age latent codes belonging to the same age group. In practice, we employ an MLP structure for its implementation, where the number of outputs is set to  $K$ .

**Face generator module.** Our face generator uses two modalities of signals as its input: a face image (real/generated) and an age latent code (sampled/predicted). For example, given

the source input face  $\mathbf{X}$  and an age latent code  $\mathbf{u}_k$ , our generator can synthesize a possible target face  $\mathbf{Y}_k = G_{img}(\mathbf{X}, \mathbf{u}_k)$ , with desired age patterns. Here, we take an encoder-decoder form for the generator’s implementation, which generally follows the previous work [6]. The impact of age latent codes on extracted facial features is realized by ”weight demodulation” [2]. The generator is encouraged to yield facial syntheses with distinct age transformation effects by conditioning on different age latent codes from the same age range. This goal is achieved by forcing the module to maximize:

$$\mathcal{L}_{div}^{img} = \mathbb{E}_{\mathbf{X}, \mathbf{u}_k} [||G_{img}(\mathbf{X}, \mathbf{u}_k^1) - G_{img}(\mathbf{X}, \mathbf{u}_k^2)||], \quad (2)$$

where  $\mathbf{u}_k^1$  and  $\mathbf{u}_k^2$  represent two different age latent codes sampled from the age stage  $k$ .

**Age latent code predictor module.** The predictor must accurately predict the corresponding age latent codes of real or generated facial images. We achieve this goal by forcing the predictor to give predictions of the age-transformed faces consistent with the sampled latent age codes used to synthesize them. This is formulated as

$$\mathcal{L}_{age}^{img} = \mathbb{E}_{\mathbf{X}, \mathbf{u}_k} [||P_{img}(G_{img}(\mathbf{X}, \mathbf{u}_k)) - \mathbf{u}_k||]. \quad (3)$$

The effects of this module are two-fold: (a) making the face generator produce results without ignoring the input age information and (b) providing necessary age-related signals to realize image reconstruction constraints. The predictor’s

structure in our realization is the concatenation of multiple convolutional layers and  $K$  parallel fully connected layers as outputs.

**Face discriminator module.** Similar to [5], [6], here we employ a multi-task learning discriminator with  $K$  output neurons. The  $k$ th branch makes binary classifications of the input face: whether the subject looks realistic and shows reasonable aging patterns at the  $k$ th age stage or not. The related adversarial learning objective is formulated as follows:

$$\mathcal{L}_{adv}^{img} = \mathbb{E}_{\mathbf{X}} [\log D_{img}(\mathbf{X})] + \mathbb{E}_{\mathbf{X}, \mathbf{u}_k} [\log D_{img}(G_{img}(\mathbf{X}, \mathbf{u}_k))]. \quad (4)$$

### B. Rectification of Facial Geometry Diversity

Experiments show that diverse age transformation effects produced by the  $DLAT_{img}$  are mainly changes of facial texture while exhibiting few variations of the facial shape. Thus, we devise a geometric version of Diverse and Lifespan Age Transformation model dubbed  $DLAT_{lmk}$ , focusing on learning the deformation of facial geometry represented by facial landmarks. Similar to its counterpart, the training process of  $DLAT_{lmk}$  also relies on four separate network components: the diverse age mapping network  $M_{lmk}$ , landmarks generator  $G_{lmk}$ , age latent code predictor  $P_{lmk}$  and the landmarks discriminator  $D_{lmk}$ . Their correlations during training are given in Fig. 1(b).

The function and implementation of  $M_{lmk}$  completely inherit from  $M_{img}$ . Regarding the landmarks generator  $G_{lmk}$ , it is used to predict offsets caused by age changes with respect to the original landmarks on the input face. To be more concrete, it takes dimension-reduced facial landmarks, achieved by applying principle component analysis (PCA) to the original data in advance as one of its inputs. Accordingly, the deformed landmarks can be obtained after conducting inverse PCA to the generator’s output estimation. The reason for these special designs is that we empirically found them favorable for generating stable results. More analysis about this will be given in Section V-E. The age latent code is another input signal for  $G_{lmk}$ . We use age codes to modulate landmark-related features through FiLM operations [52]. Since the inputs and outputs of  $G_{lmk}$ ,  $P_{lmk}$  and  $D_{lmk}$  are all vector-formed representations of face landmarks, their network implementations are simple multi-layer perceptrons (MLPs). Relevant objectives, i.e.,  $\mathcal{L}_{div}^{lmk}$ ,  $\mathcal{L}_{age}^{lmk}$  and  $\mathcal{L}_{adv}^{lmk}$  are easy to deduce by replacing the image input with PCA-processed landmarks in their respective counterparts.

### C. Consistency Constraints of Race and Pose

Experiments show that simply encouraging the model to pursue diversity in age transformation usually leads to unreasonable results. For instance, given an input face with white skin, the  $DLAT_{img}$  occasionally generates age-transformed faces with black skin. Fed by a set of frontal facial landmarks, the  $DLAT_{lmk}$  sometimes yields deformed landmarks watching towards the sides. All these abnormal syntheses are contrary to our expectations: diverse and reasonable age transformation effects without modifying other facial attributes. In order

to avoid unreasonable diversity, we propose race and pose consistency constraints for two age transformation systems, respectively.

The race consistency constraint for  $DLAT_{img}$  can be written as,

$$\mathcal{L}_{rac} = \begin{cases} 0, & \text{if } R(\mathbf{X}) = R(\mathbf{Y}) \\ \mathbb{E}_{\mathbf{X}, \mathbf{Y}} (1 - c), & \text{else} \end{cases}, \quad (5)$$

where  $R$  is a third-party race estimator [53] that predicts a confidence (also called probability) distribution of the input face belonging to the considered race list. Here,  $R(\mathbf{X}) = R(\mathbf{Y})$  means the source and generated faces are classified into the same race class, and  $c$  denotes the estimated confidence of the generated face categorized into the particular race class of the source face. Through minimizing  $\mathcal{L}_{rac}$ , the  $DLAT_{img}$  is forced to produce synthetic faces having the same ethnicity as the source. On the other hand, the plain philosophy behind our pose consistency constraint is to ensure that the poses of the input facial landmarks and deformed ones generated by the  $DLAT_{lmk}$  model are identical. We first construct a reference set composed of fixed and separated 3D points to obtain the pose approximation of those landmarks. Note that these points can be randomly chosen while satisfying the requirements of a pre-defined amount and mutual separability. Then, we pick an equal number of landmark pairs with the same locations on the face structure (e.g., the tip of the nose) from real and synthetic facial landmarks, constituting relevant landmark subsets. Finally, we compute the transformation from those 3D reference points to 2D selected landmarks with mature Perspective-n-Point (PnP) algorithms and regard it as the pose approximation corresponding to the current type of landmarks. The pose consistency restriction can then be formulated as follows:

$$\mathcal{L}_{pos} = \mathbb{E}_{L_X, L_Y} [||P(L_X) - P(L_Y)||], \quad (6)$$

where  $P(L_X)$  and  $P(L_Y)$  denote pose calculation on real and generated facial landmarks, respectively.

### D. Training Objectives

**Compound identity preservation.** The original and synthesized faces need to seem like the same person perceptually, but only with differences in aging patterns. To achieve this goal, we design compound identity preservation losses to regularize the training processes of two age transformation models. Specifically, we employ three objectives for the  $DLAT_{img}$  to make regularization at pixel and feature levels. The first one is image cycle consistency, which is formulated as,

$$\mathcal{L}_{cyc}^{img} = \mathbb{E}_{\mathbf{X}, \mathbf{Y}} [||\mathbf{X} - G_{img}(\mathbf{Y}, P_{img}(\mathbf{X}))||]. \quad (7)$$

The second one is perceptual consistency [54], written as,

$$\mathcal{L}_{ppc} = \mathbb{E}_{\mathbf{X}, \mathbf{Y}} [||F_{vgg}(\mathbf{X}) - F_{vgg}(G_{img}(\mathbf{Y}, P_{img}(\mathbf{X})))||], \quad (8)$$

where  $F_{vgg}$  computes feature maps from the first four layers of a pre-trained VGG [55]. The third one is identity feature consistency, which is defined as,

$$\mathcal{L}_{idc} = \mathbb{E}_{\mathbf{X}, \mathbf{Y}} [1 - \cos(E_{fr}(\mathbf{X}), E_{fr}(\mathbf{Y}))], \quad (9)$$

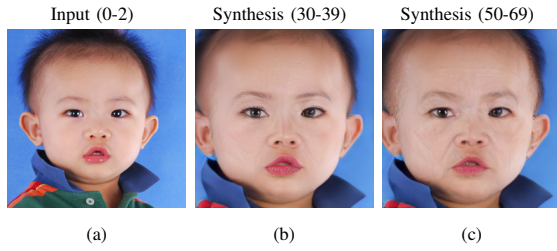


Fig. 2. Examples of poor age transformation synthesis that apparently contradict universal aging rules on human faces. However, these generations are appreciated when simply considering high face verification rates (91.27% between (a) and (b), 91.58% between (a) and (c), measured by Face++ API for face comparing) indicating more reasonable preservation of identity information across ages.

where  $E_{fr}$  denotes using a pre-trained face recognition network (arcface [56] in our implementation) to calculate identity-related feature vectors with unit norm lengths, and  $\cos(\cdot, \cdot)$  means calculating cosine similarity between the input vector pair.

We devise two objectives for the  $DLAT_{lmk}$  model to preserve identity information. The first loss is the landmark cycle consistency  $\mathcal{L}_{cyc}^{lmk}$ , which has the same form as the  $\mathcal{L}_{cyc}^{img}$ . The other loss is personal characteristic consistency, which is defined as,

$$\mathcal{L}_{pcc} = \mathbb{E}_{L_X, L_Y} [1 - \cos(L_X - \bar{L}^r, L_Y - \bar{L}^t)]. \quad (10)$$

In this formula,  $L_X$  and  $L_Y$  are genuine and generated landmarks, and  $\bar{L}^r$  and  $\bar{L}^t$  are the averages of all real landmarks from the training datasets belonging to the source and target age groups, respectively. Through minimizing  $\mathcal{L}_{pcc}$ , the  $DLAT_{lmk}$  network is demanded to maintain the personal characteristics of the human subject in facial geometry. The reasonability behind this loss is straightforward. For example, if a child is born with a pair of bigger eyes than most children, this characteristic will remain for the rest of the corresponding subject's life.

**Full objective function.** For  $DLAT_{img}$ , the whole losses used to supervise the model's training are:

$$\begin{aligned} \mathcal{L}_{img} = & \lambda_1 \mathcal{L}_{adv}^{img} + \lambda_2 \mathcal{L}_{div}^{img} + \lambda_3 \mathcal{L}_{age}^{img} + \lambda_4 \mathcal{L}_{cyc}^{img} + \\ & \lambda_5 \mathcal{L}_{rac} + \lambda_6 \mathcal{L}_{pcc} + \lambda_7 \mathcal{L}_{idc}. \end{aligned} \quad (11)$$

On the other hand, total objectives for  $DLAT_{lmk}$  can be summarized as:

$$\begin{aligned} \mathcal{L}_{lmk} = & \lambda_8 \mathcal{L}_{adv}^{lmk} + \lambda_9 \mathcal{L}_{div}^{lmk} + \lambda_{10} \mathcal{L}_{age}^{lmk} + \lambda_{11} \mathcal{L}_{cyc}^{lmk} + \\ & \lambda_{12} \mathcal{L}_{pos} + \lambda_{13} \mathcal{L}_{pcc}. \end{aligned} \quad (12)$$

Note that these two networks are learned separately during the training stage. When it goes into the inference stage,  $DLAT_{img}$  can work independently or integrate with  $DLAT_{lmk}$  through image warping operations, which forms our enhanced diverse and lifespan age transformation model,  $DLAT^+$ .

#### IV. METRIC FOR IDENTITY DEVIATION UNDER AGE GAPS

To achieve the quantitative performance of an age transformation method, an important aspect is evaluating its ability to preserve the subject's identity information appropriately. Previous works [9], [12]–[14] usually resort to a well-performed face verification model and use it to calculate

the average similarity between original and age-transformed faces. Then, a higher mean similarity score is regarded as a better result. However, according to our common sense, the appearances of the same person in different age stages show variations: they look similar but not identical. More specifically, the perceptual similarity between two faces of a particular human subject decreases as their age gap increases. Therefore, the conventional metric for identity preservation in the age-transformation scenario is unsuitable. Another piece of evidence is given in Fig. 2, where the synthetic faces only demonstrate textural aging patterns. Nevertheless, those two absurd age transformation results are appreciated under the blind awarding of high face verification rates.

In order to quantitatively investigate how the identity similarities of a face pair change with the varying age deviation between them in reality, we make analyses on the public FG-NET [57] and Cross-Age Face [9] datasets. These two datasets contain 602 subjects in total, and each subject has 8.3 facial images on average captured under different age stages. Following [5], we first divide the whole life cycle into ten consecutive and non-overlapped age groups, namely 0-2 (A), 3-6 (B), 7-9 (C), 10-14 (D), 15-19 (E), 20-29 (F), 30-39 (G), 40-49 (H), 50-69 (I), and 70+ (J). Then, for faces of each subject in these datasets, we use the face verification model provided by the Face++ API [58] to calculate similarity scores of all image pairs. These scores are further categorized and averaged according to source and target age group pairs. Statistics for them summarized in Fig. 3 clearly show that trends of calculated identity similarities between face pairs of the same person with different age conditions align with universal face-aging rules. For details of numerical values in these sub-figures, please refer to Table VI in supplementary materials.

With these ground-truth distributions of identity similarity, we propose our metric for **Identity Deviation under Age Gaps** (IDAG), the definition of which is:

$$IDAG = \frac{1}{N \times M} \sum_{i=1}^N \sum_{j=1}^M |\hat{s}(\mathbf{X}_i, \mathbf{Y}_i^j) - \bar{s}_i^j| \times 100\%, \quad (13)$$

where  $N$  is the number of source faces involved and  $M$  is the number of age groups considered (thus  $1 \leq M \leq 10$ ). In addition,  $\hat{s}(\mathbf{X}_i, \mathbf{Y}_i^j)$  denotes the identity similarity predicted by the Face++ API between a face pair, the source one  $\mathbf{X}_i$  and its corresponding synthesis  $\mathbf{Y}_i^j$  in the predefined  $j$ th age phase. The notation  $\bar{s}_i^j$  represents the mean similarity among real faces captured from the same persons under the source age group ( $\mathbf{X}_i$  belongs to) and the target age group ( $\mathbf{Y}_i^j$  is located in), which has been computed and collected in Fig. 3.

## V. EXPERIMENTS

### A. Experimental Settings

**Datasets.** We use images from the FFHQ-Aging dataset [59] for models' training and evaluation purposes. The whole life duration is divided into ten separate age clusters based on the joint change of facial texture and shape at different age stages. However, only those clusters with sizes above a certain amount are chosen, considering the requirement of large numbers of

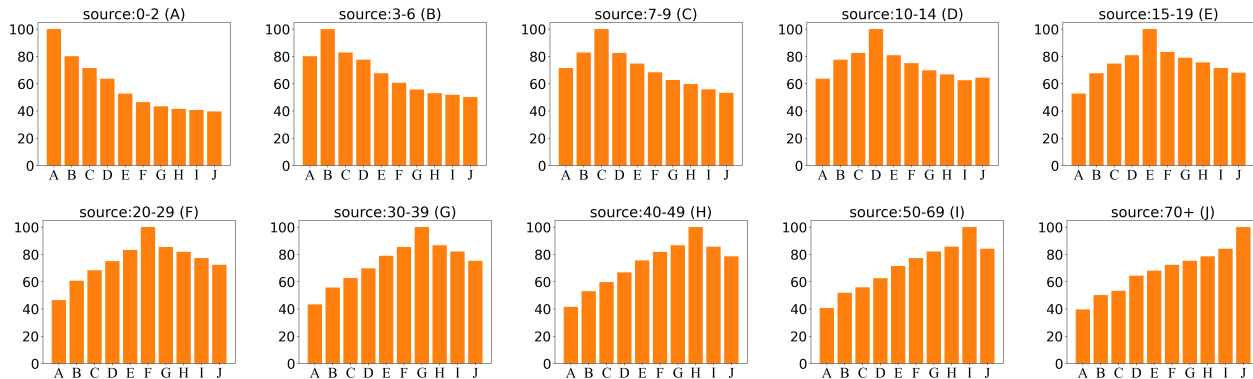


Fig. 3. Statistical analysis on two large face-aging datasets about average variation trends of identity information across ages. For each portrait of a specific age condition (the source age stage), we take it as the anchor and compare its identity similarities with faces from the same subject at identical or different phases. Similarity scores are calculated via the Face++ API. The symbols A to J denote ten consecutive age groups.

training samples from the neural network. Eventually, there are 14,232 male and 14,066 female faces selected for training, 198 male and 205 female faces for testing. Facial images in the training set come from six age groups: 0-2, 3-6, 7-9, 15-19, 30-39, and 50-69. In addition, the FG-NET [57] (1,002 faces of 82 individuals) and Cross-Age Face [9] (4000 faces of 520 individuals) datasets are leveraged to obtain the ground-truth mean similarity components of our IDAG metric. An important property of these two datasets is that each human subject included has multiple facial captures at different age phases, while other datasets just provide facial photos of each certain person within a single age stage.

**Baselines.** We take two kinds of methods into comparison. The first category includes state-of-the-art approaches particularly designed to deal with the lifespan age transformation task. They are LATS [5], DLFS [6], SAM [8], CUSP [10], and AgeTransGAN [9]. Methods in the second category contain InterFaceGAN [47] and Latent-Transformer [60], designed to realize general image attributes editing by manipulating relevant latent codes in the latent space of a StyleGAN2 [2] pretrained on FFHQ [4] human face dataset. We employ the HyperStyle [61] for InterFaceGAN and pSp [62] for Latent-Transformer to obtain latent codes of source facial images. A noteworthy limitation of this type of image editing technique is that although it can produce a younger or older synthesis of the input face, precise control of the target age condition is inaccessible.

**Implementation Details.** Following the practices in [5], [6], we train two separate models of our DLAT<sup>+</sup>, one for males and the other for females. In addition, during the pre-processing stage, all images in the training set are resized to 256 × 256 resolution, and the background is removed using semantic masks provided by the dataset. An off-the-shelf detector [63] is used to predict 81 landmarks for the given faces. All our models are learned on a single RTX 3090 GPU with a batch size of 2. We employ the Adam algorithm [64] for parameter optimization, with an initial learning rate set to 0.001 and decayed by 0.1 at the 50th and 100th epochs, while the whole training lasts for 300 epochs. The length of age latent codes in DLAT<sub>img</sub> and DLAT<sub>lmk</sub> are set to 256 and 64, respectively. Regarding those hyper-parameters from

$\lambda_1$  to  $\lambda_{13}$  in Eqs. 11 and 12, we assign values of 1, 0.6, 10, 10, 1, 1, 0.2, 35, 2, 50, 10, 1, and 10 to them empirically.

**Evaluation Metrics.** We evaluate methods for lifespan age transformation through automatic evaluation and user study. In automatic assessment, the proposed metric IDAG is used to measure the rationality of identity variation caused by age changes. Following the practices in [65], [66], the LPIPS [67] is calculated among a fixed number of synthesized faces in the same age cluster, where a higher value indicates a better diversity of face aging results. Besides, we employ the face detection API provided by Baidu AI Cloud [68] to predict ages of synthetic faces and compute their absolute numerical differences with respect to corresponding target age groups we want to synthesize. These differences are summed up and then averaged, the derived final result is referred to as the mean absolute error (MAE) in age transformation.

### B. Quantitative Comparisons

Since general image editing methods do not support age-related signals as the input, for the InterFaceGAN and Latent-Transformer involved, it is impossible to compute the age transformation error. However, we can use a well-performed age estimator to predict the corresponding age stages to which their synthesized faces belong. Furthermore, syntheses within the considered age clusters can be selected and compared with original input faces under the proposed IDAG metric. Quantitative results in terms of the identity deviation rationality and age transformation error yielded by our full model, DLAT<sup>+</sup>, and other methods are tabulated in Tables I and II.

Results in table I show that: 1) Overall, it is rather difficult for current age transformation methods to fit the changing rules of human facial identity caused by age transition; 2) Approaches particularly designed for lifespan age transformation task demonstrate more reasonable variations of facial identity information across ages compared to those universal image editing techniques. Recall that the latter ones realize facial attribute modification by manipulating the corresponding latent codes in a pre-trained GAN space. Seeking to be capable of editing as many kinds of facial attributes as possible, this feature space eventually obtains a balance between feature

TABLE I

COMPARISON OF IDENTITY VARIATION RATIONALITY BETWEEN SOURCE AND SYNTHETIC FACES

Source age \ Method	0-2	3-6	7-9	15-19	30-39	50-69
	IDAG↓					
LATS [5]	85.94	39.66	54.76	45.75	67.13	87.45
DLFS [6]	62.09	39.42	49.02	42.76	61.56	56.00
SAM [8]	141.93	88.44	83.44	69.74	92.60	90.10
CUSP [10]	114.03	45.04	33.53	<b>14.96</b>	<b>24.60</b>	31.35
AgeTransGAN [9]	175.37	122.79	110.96	92.00	110.22	128.17
InterFaceGAN [47]	131.85	110.87	95.03	72.28	103.43	70.83
Latent-Transformer [60]	156.32	130.28	87.35	88.75	106.21	100.34
DLAT <sup>+</sup> (ours)	<b>47.30</b>	<b>29.83</b>	<b>31.89</b>	18.80	29.20	<b>29.36</b>

TABLE II

COMPARISON OF AGE TRANSFORMATION ERROR BETWEEN TARGET AND SYNTHETIC AGE CONDITIONS

Target age \ Method	0-2	3-6	7-9	15-19	30-39	50-69
	MAE↓					
LATS [5]	3.01	4.55	6.74	11.50	5.20	9.86
DLFS [6]	2.29	4.57	6.27	10.19	5.03	10.50
SAM [8]	6.20	5.83	6.86	8.08	4.81	<b>6.66</b>
CUSP [10]	<b>0.84</b>	2.73	5.44	8.57	18.93	11.90
AgeTransGAN [9]	5.95	8.22	11.16	11.96	9.06	17.57
DLAT <sup>+</sup> (ours)	1.41	<b>2.59</b>	<b>5.11</b>	<b>8.03</b>	<b>4.50</b>	8.33

disentanglement and editability. Because of the partial entanglement between identity and age attributes, the editing of facial age will incur the unwanted change of identity attribute; 3) In age clusters of 15-19 and 30-39, the performance of our method closely follows the best approaches. Remarkably, we surpass the second-best competitors by 23.8%, 24.3%, 4.9%, and 6.3% when the source age groups of input faces are 0-2, 3-6, 7-9, and 50-69, respectively. Note that when the input faces fall into those age ranges located at the start or end of the life cycle, the age gaps between them and corresponding syntheses covering the left age stages are larger than those cases that source faces belonging to the middle age groups. Results indicate that we can preserve the subject’s identity more properly than others when the age transformation span is long. This superiority should be attributed to the compound losses proposed for identity preservation (see Section III-D).

Table II reveals that: 1) Given the six age groups as the synthesis target, it is easier for current age-changing algorithms to generate age-related patterns in early stages (0-9); however, it is more difficult to simulate old conditions. A possible reason for this phenomenon is that human faces widely undergo dramatic changes in facial shape during the early stage of life but relatively mild variations in texture after that period. Existing methods tend to be better at learning and modeling apparent differences than subtle ones; 2) our approach produces the lowest age transformation error in the middle four age ranges considered (3-6, 7-9, 15-19, and 30-39), outperforming the closest followers by 5.1%, 6.1%, 0.6% and 6.4%. While in the other two age groups, we also have competitive performance.

### C. Qualitative and Subjective Comparisons

Visualization of typical age-transformed results generated by all methods involved in comparison can be found in Figs. 4 and 12 in supplementary materials. These syntheses intuitively present the characteristics of each technique. In alignment with the quantitative evaluation results, approaches devised especially for facial age transformation generally yield better-aging effects than common image editing methods. Checking the generations from InterFaceGAN and Latent-Transformer, we find several problems: 1) there are apparent changes in the subject’s identity across ages; 2) Artifacts arise above the segmented facial regions where they should be empty and unwanted ornaments (such as glasses) come out; 3) Unnatural facial syntheses occur when the target age conditions are located in childhood. We think the weak decoupling of features related to distinct facial attributes in the pre-trained GAN’s latent space and the over-reliance on the prior knowledge it provides jointly lead to the aforementioned issues. Drawbacks also exist among those specific algorithms designed for aging simulation. For instance, unexpected glasses appear in the synthetic female faces produced by LATS, as well as artifacts from CUSP and DLFS. In addition, SAM usually generates abnormal texture changes (pay attention to the regions around the eyes), whereas AgeTransGAN always yields nearly the same facial shapes throughout the lifespan, which echoes its poor records in Table I. In contrast, faces synthesized by our method exhibit more reasonable aging patterns and consistent personal characteristics across ages. Besides, our approach shows an interesting property: it can partially eliminate possible inappropriate illumination impacts on the captured faces (such as overexposure or underexposure) and restore the subject’s original skin color in the corresponding facial syntheses with age progression or regression. We attribute this to the additional advantage of explicitly forcing race consistency between original and synthesized faces.

On the other hand, we conduct subjective evaluations of our method and other compared approaches through the user study. To be more specific, 20 participants are asked to score age transformation syntheses generated by approaches in comparison. The subjective assessment involves six perspectives: *identity consistency*, *shape deformation plausibility*, *texture transformation plausibility*, *synthetic image quality*, *age transformation error*, and *diversity*. Note that these aspects are mutually orthogonal. Statistics in Table III demonstrate that our algorithm obtains the best performance under all evaluating viewpoints, meaning better approval degrees between human beings’ perceptual experience of face aging rules and our aging generations.

### D. Comparisons of Age Transformation Diversity

Quantitative evaluations about the age transformation diversity of our method and other approaches are tabulated in Table IV. The results show that our algorithm beats those opponents by several orders of magnitude under the LPIPS metric. After checking the synthesized faces under every specific target age group generated by those approaches, we could hardly find subtle variations among their corresponding generations. In

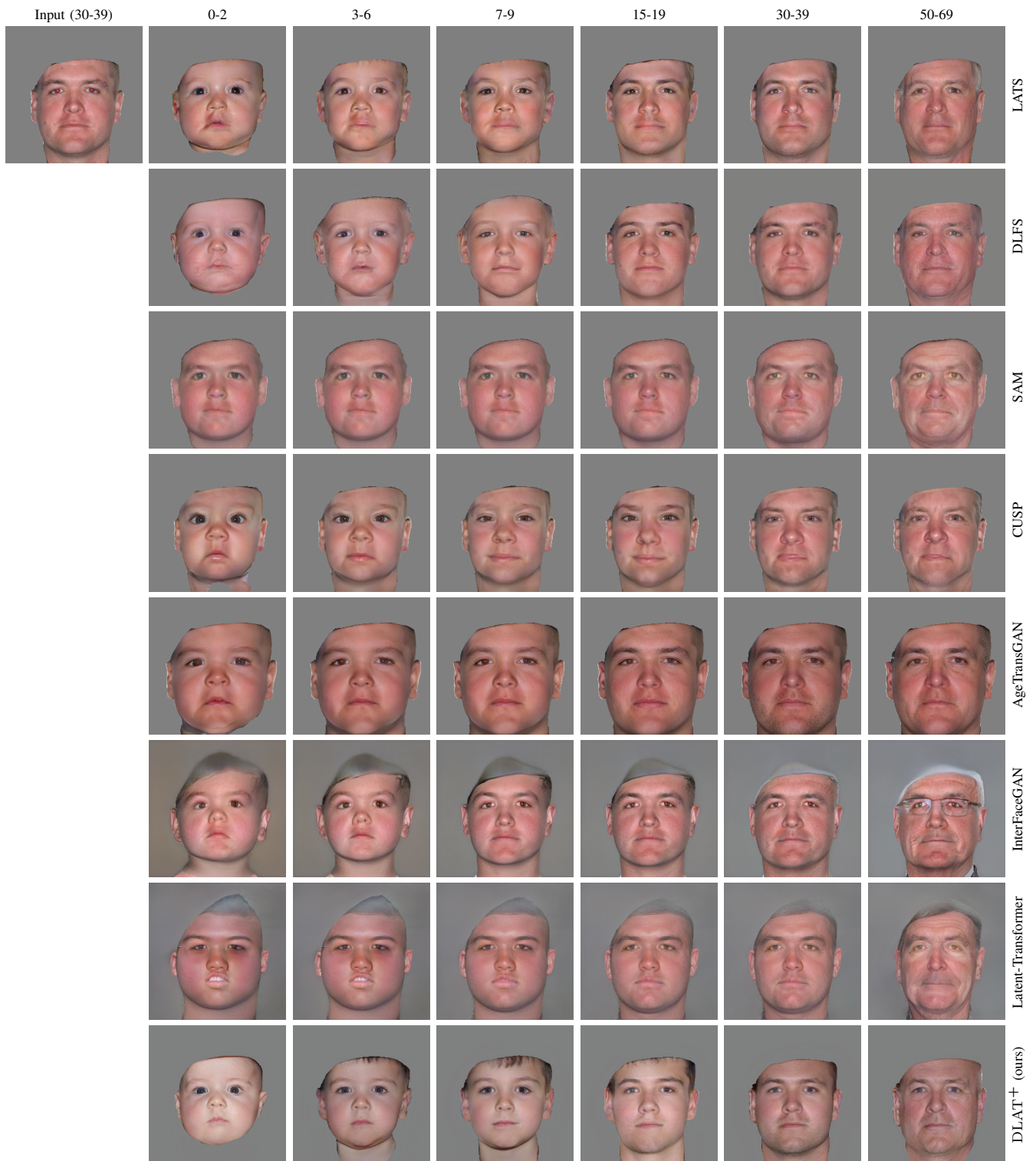


Fig. 4. Visual comparison among lifespan age transformation results of the given male subject, which are synthesized by LATS, DLFS, SAM, CUSP, AgeTransGAN, InterFaceGAN, Latent-Transformer, and our DLAT<sup>+</sup>.

TABLE III  
USER STUDY OF AGE TRANSFORMATION RESULTS

Method	Identity consistency $\uparrow$	Shape deformation plausibility $\uparrow$	Texture deformation plausibility $\uparrow$	Synthetic image quality $\uparrow$	Age transformation error $\downarrow$	Age transformation diversity $\uparrow$
LATS [5]	67.37	70.47	64.21	63.16	4.2	35.26
DLFS [6]	73.16	73.68	76.84	72.63	3.4	33.68
SAM [8]	54.21	40.87	51.05	61.58	17.3	34.74
CUSP [10]	44.21	42.11	35.79	39.47	15.4	25.79
AgeTransGAN [9]	54.74	31.05	37.37	52.11	24.6	33.16
InterFaceGAN [47]	50.00	57.37	62.11	60.00	23.2	38.95
Latent-Transformer [60]	32.10	35.79	34.21	31.58	7.1	31.58
DLAT <sup>+</sup> (ours)	<b>83.68</b>	<b>79.85</b>	<b>79.47</b>	<b>78.37</b>	<b>2.6</b>	<b>74.73</b>

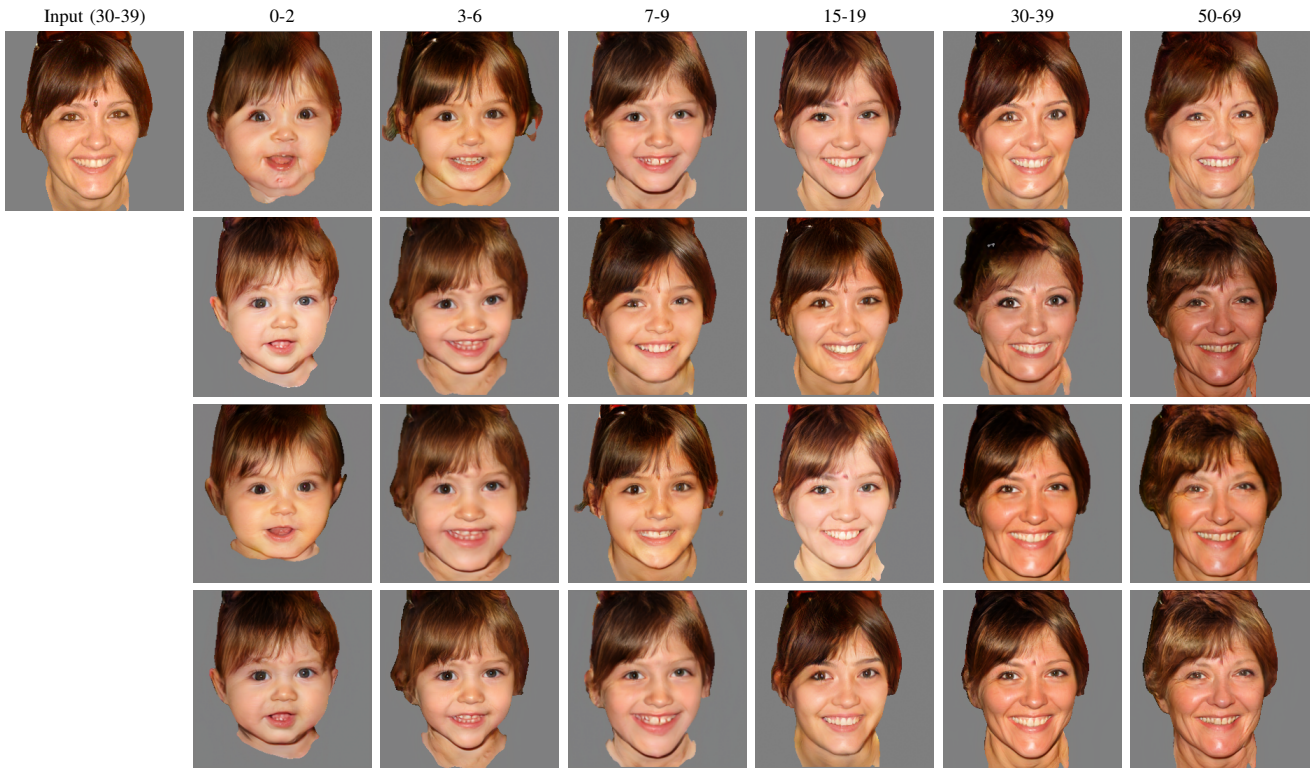


Fig. 5. Visualization of diverse age transformation results across the life cycle, generated by applying our full method to a female subject.

other words, these methods only yield deterministic aging effects. However, according to common sense, a person’s appearance at any age timestamp should have infinite possibilities. On the other hand, representative visualization results produced by our technique are shown in Figs. 5 and 11 in supplementary materials. These synthesized faces show that our full model, DLAT<sup>+</sup>, is capable of generating photo-realistic and vivid age-progressed or regressed faces of the input portrait. At the same time, the diversity is prominently reflected in facial texture and shape levels. This exclusive advantage compared to other age transformation methods should be attributed to our special design of the diverse mechanism in the age-conditioned synthetic procedure and the proposed facial geometry rectification scheme based on face landmarks, accompanied by multiple constraints on race, pose and identity consistency to control the aging diversity within a reasonable range.

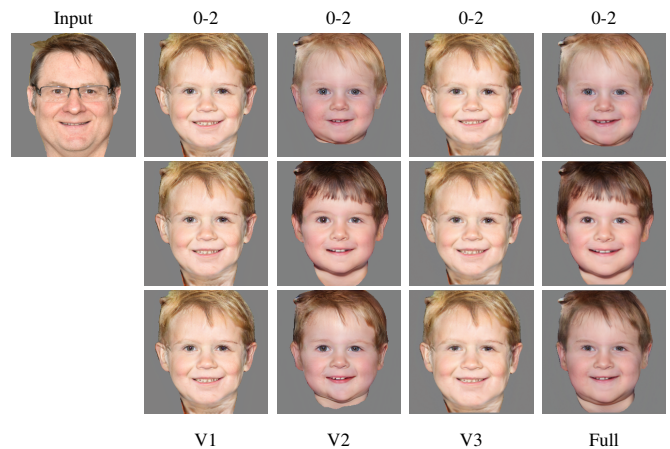


Fig. 6. Visual comparison among results of transforming the input face to the age range from 0 to 2. V2 denotes the DLAT<sub>img</sub>, while V1 is its variant through ablating the diversity mechanism. V3 represents the version of V1 plus DLAT<sub>lmk</sub>. The full model is the integration between DLAT<sub>img</sub> and DLAT<sub>lmk</sub>.

TABLE IV  
COMPARISON OF AGE TRANSFORMATION DIVERSITY UNDER CERTAIN TARGET AGE GROUPS

Method	Target age	0-2	3-6	7-9	15-19	30-39	50-69
	LPIPS↑						
LATS [5]		$2.1 \times 10^{-2}$	$1.7 \times 10^{-2}$	$1.3 \times 10^{-2}$	$1.3 \times 10^{-2}$	$1.4 \times 10^{-2}$	$1.5 \times 10^{-2}$
DLFS [6]		$1.6 \times 10^{-2}$	$1.5 \times 10^{-2}$	$9.7 \times 10^{-3}$	$7.3 \times 10^{-3}$	$5.6 \times 10^{-3}$	$9.4 \times 10^{-3}$
SAM [8]		$9.2 \times 10^{-5}$	$9.2 \times 10^{-5}$	$9.0 \times 10^{-5}$	$8.8 \times 10^{-5}$	$8.9 \times 10^{-5}$	$9.6 \times 10^{-5}$
CUSP [10]		$2.0 \times 10^{-2}$	$2.1 \times 10^{-2}$	$2.2 \times 10^{-2}$	$2.1 \times 10^{-2}$	$1.6 \times 10^{-2}$	$2.0 \times 10^{-2}$
AgeTransGAN [9]		$1.7 \times 10^{-2}$	$1.6 \times 10^{-2}$	$1.3 \times 10^{-2}$	$1.8 \times 10^{-2}$	$1.7 \times 10^{-2}$	$1.8 \times 10^{-2}$
InterFaceGAN [47]		$3.1 \times 10^{-2}$	$2.7 \times 10^{-2}$	$3.4 \times 10^{-2}$	$2.3 \times 10^{-2}$	$2.5 \times 10^{-2}$	$2.7 \times 10^{-2}$
Latent-Transformer [60]		$2.8 \times 10^{-2}$	$3.2 \times 10^{-2}$	$2.3 \times 10^{-2}$	$2.8 \times 10^{-2}$	$2.9 \times 10^{-2}$	$3.3 \times 10^{-2}$
DLAT <sup>+</sup> (ours)		<b><math>2.0 \times 10^{-1}</math></b>	<b><math>1.4 \times 10^{-1}</math></b>	<b><math>1.3 \times 10^{-1}</math></b>	<b><math>1.7 \times 10^{-1}</math></b>	<b><math>1.8 \times 10^{-1}</math></b>	<b><math>1.8 \times 10^{-1}</math></b>

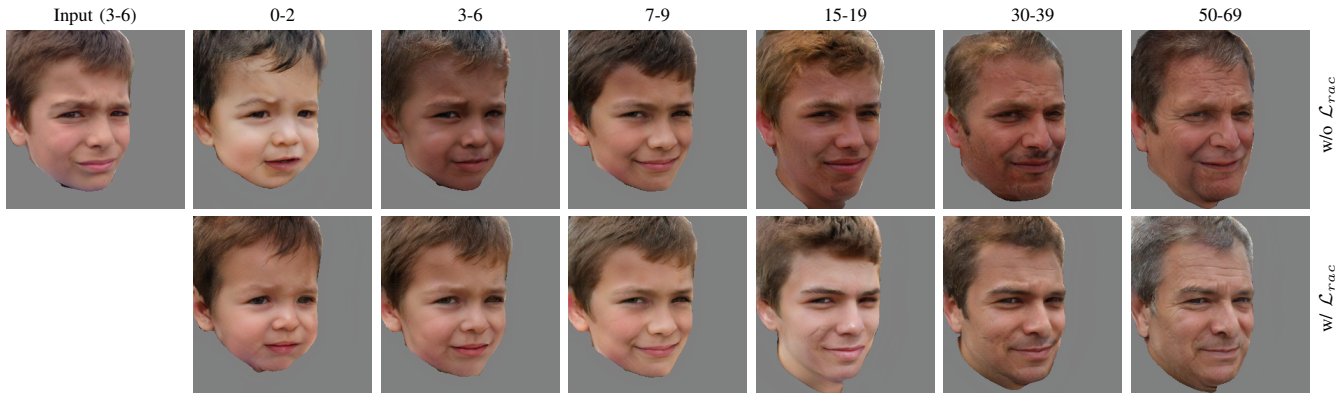


Fig. 7. Generations comparison of training our DLAT<sub>img</sub> without (w/o) or with (w) the race consistency constraint.

TABLE V  
ABLATION STUDY OF DIVERSITY MECHANISMS IN OUR METHOD

Method	Target age	0-2	3-6	7-9	15-19	30-39	50-69
	LPIPS↑						
V1		0.016	0.015	0.010	0.007	0.006	0.009
V2		0.106	0.089	0.071	0.083	0.118	0.111
V3		0.077	0.059	0.054	0.081	0.084	0.086
Full		<b>0.204</b>	<b>0.143</b>	<b>0.132</b>	<b>0.166</b>	<b>0.184</b>	<b>0.182</b>

E. Ablation Studies

**Hybrid diversity mechanism.** We use three variants of our method to explore the impact of components in the proposed compounded diversity design. Our DLAT<sub>img</sub> is regarded as the second variant (V2). We obtain the first version (V1) based on it by removing the age latent code predictor module and related losses. As a result, the implementation of this version is close to DLFS. Since DLAT<sub>lmk</sub> cannot work independently, we combine it with the V1 model, forming the third variant (V3). From the generations illustrated in Fig. 6, we observe that V1 produces deterministic facial rejuvenation. After warping its syntheses with the transformation provided by DLAT<sub>lmk</sub>, slight but noticeable variations show up on the facial shape (pay attention to the difference of face counters yielded by V3). On the other hand, directly introducing a diversity mechanism to V1 at the pixel and feature vector levels (i.e., V2) mainly brings uncertainty to the facial texture. Our full model, the integration of DLAT<sub>img</sub> and DLAT<sub>lmk</sub>, demonstrates the most comprehensive age transformation di-

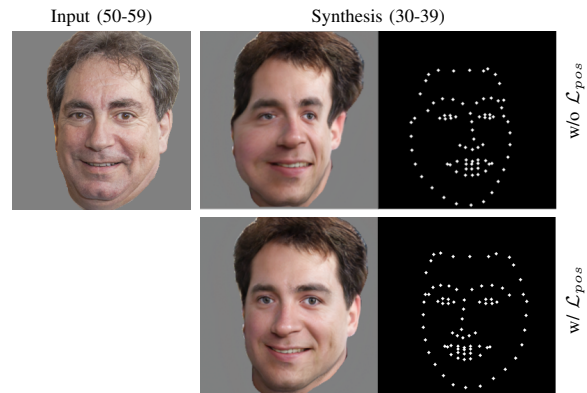


Fig. 8. Generations comparison of training our DLAT<sub>lmk</sub> without (w/o) or with (w) the pose consistency constraint.

versity, including textural and structural aspects. Relevant objective results in Table V further validate the above visual findings.

**Pose and race conformance constraints.** The race consistency constraint is conducted on DLAT<sub>img</sub> by using  $\mathcal{L}_{rac}$  loss in its training process. Visual results shown in Fig. 7 demonstrate that without this constraint, the network tends to overly change the skin color to maximize the age transformation diversity, causing unwanted falsification of the subject's ethnic attribute. In contrast, employing this restriction helps the DLAT<sub>img</sub> avoid possible race-changing problems. On the other hand, the pose consistency demand is made to DLAT<sub>lmk</sub>

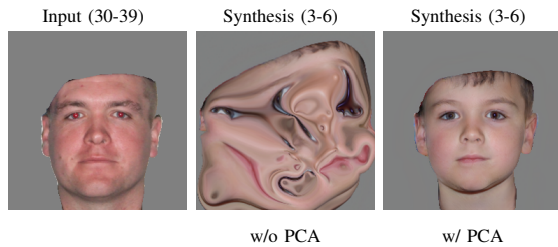


Fig. 9. Generations comparison of implementing our  $DLAT_{lmk}$  without (w/o) or with (w/) PCA feature dimension reduction.

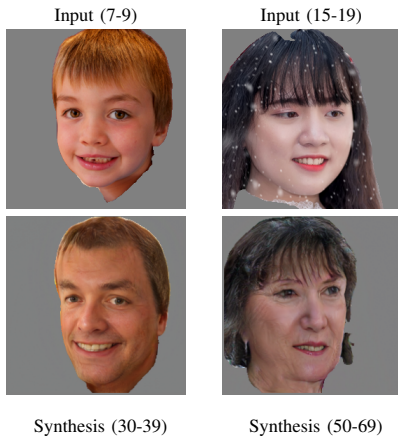


Fig. 10. Representative failure generations yielded by our  $DLAT^+$ . These syntheses show grotesqueness in facial structures.

with  $\mathcal{L}_{pos}$  loss, aiming at preventing the network from changing the input person’s pose to obtain higher variations of landmarks syntheses. Comparison results depicted in Fig. 8 verify its effectiveness.

**PCA on facial landmarks.** In the realization of  $DLAT_{lmk}$ , we apply PCA to the extracted 2D landmarks and obtain their corresponding 1D feature points. Subsequent feature modulation based on age conditions and diversity mechanism is conducted on these dimensionality-reduced feature points rather than the original landmarks. This operation is because we empirically found it favors the preservation of spatial relationships among individual facial landmarks, while directly processing raw landmarks usually incurs generations with broken spatial structure. A visual evidence is given in Fig. 9.

## VI. CONCLUSION

This paper presents the first method to synthesize diverse and plausible age transformations on human faces while allowing the target age stages to be chosen throughout the lifetime. Benefiting from the specially designed mechanism, various aging effects simultaneously manifest in the facial texture and shape aspects. Moreover, based on the golden standard summarized from abundant sequential faces of the same persons but at different ages, we also introduce the first metric for assessing the rationality of identity variations between input portraits and corresponding age-regressed or progressed syntheses. Although our technique proves its uniqueness and effectiveness in extensive experiments, failures

occasionally appear, and some typical samples are given in Fig. 10. For instance, if the reference portrait is a side face with a relatively large yaw angle relative to the frontal pose, the output generations occasionally seem strange in facial structure. To alleviate this problem, involving prior knowledge of complete 3D heads may be favorable. In addition, conducting age transformation based on video inputs is a valuable but rarely explored direction, the challenges of which mainly lie in achieving consistent aging effects across synthetic frames. We leave this exploration to our future work.

## REFERENCES

- [1] T. Karras, S. Laine, and T. Aila, “A style-based generator architecture for generative adversarial networks,” in *Proceedings of the IEEE Conference on Computer Vision and Pattern Recognition (CVPR)*, 2019, pp. 4401–4410.
- [2] T. Karras, S. Laine, M. Aittala, J. Hellsten, J. Lehtinen, and T. Aila, “Analyzing and improving the image quality of StyleGAN,” in *Proceedings of the IEEE Conference on Computer Vision and Pattern Recognition (CVPR)*, 2020, pp. 8110–8119.
- [3] T. Karras, M. Aittala, S. Laine, E. Härkönen, J. Hellsten, J. Lehtinen, and T. Aila, “Alias-free generative adversarial networks,” in *Proceedings of the Advances in Neural Information Processing Systems (NeurIPS)*, 2021, pp. 852–863.
- [4] The FFHQ dataset. Accessed Dec. 26, 2023. [Online]. Available: <https://github.com/NVlabs/ffhq-dataset>
- [5] R. Or-El, S. Sengupta, O. Fried, E. Shechtman, and I. Kemelmacher-Shlizerman, “Lifespan age transformation synthesis,” in *Proceedings of the European Conference on Computer Vision (ECCV)*, 2020, pp. 739–755.
- [6] S. He, W. Liao, M. Y. Yang, Y.-Z. Song, B. Rosenhahn, and T. Xiang, “Disentangled lifespan face synthesis,” in *Proceedings of the IEEE International Conference on Computer Vision (ICCV)*, 2021, pp. 3877–3886.
- [7] X. Hou, X. Zhang, H. Liang, L. Shen, and Z. Ming, “Lifelong age transformation with a deep generative prior,” *IEEE Transactions on Multimedia (TMM)*, vol. 25, pp. 3125–3139, 2022.
- [8] Y. Alaluf, O. Patashnik, and D. Cohen-Or, “Only a matter of style: Age transformation using a style-based regression model,” *ACM Transactions on Graphics (TOG)*, vol. 40, no. 4, pp. 1–12, 2021.
- [9] G.-S. Hsu, R.-C. Xie, Z.-T. Chen, and Y.-H. Lin, “AgeTransGAN for facial age transformation with rectified performance metrics,” in *Proceedings of the European Conference on Computer Vision (ECCV)*, 2022, pp. 580–595.
- [10] G. Gomez-Trenado, S. Lathuilière, P. Mesejo, and Ó. Cerdón, “Custom structure preservation in face aging,” in *Proceedings of the European Conference on Computer Vision (ECCV)*, 2022, pp. 565–580.
- [11] L. Liu, S. Wang, L. Wan, and H. Yu, “Multimodal face aging framework via learning disentangled representation,” *Journal of Visual Communication and Image Representation*, vol. 83, p. 103452, 2022.
- [12] Z. Li, R. Jiang, and P. Aarabi, “Continuous face aging via self-estimated residual age embedding,” in *Proceedings of the IEEE Conference on Computer Vision and Pattern Recognition (CVPR)*, 2021, pp. 15008–15017.
- [13] Y. Liu, Q. Li, and Z. Sun, “Attribute-aware face aging with wavelet-based generative adversarial networks,” in *Proceedings of the IEEE Conference on Computer Vision and Pattern Recognition (CVPR)*, 2019, pp. 11 877–11 886.
- [14] H. Yang, D. Huang, Y. Wang, and A. K. Jain, “Learning continuous face age progression: A pyramid of GANs,” *IEEE Transactions on Pattern Analysis and Machine Intelligence (TPAMI)*, vol. 43, no. 2, pp. 499–515, 2019.
- [15] Y. Liu, Q. Li, Z. Sun, and T. Tan, “A<sup>3</sup>GAN: an attribute-aware attentive generative adversarial network for face aging,” *IEEE Transactions on Information Forensics and Security (TIFS)*, vol. 16, pp. 2776–2790, 2021.
- [16] J. T. Todd, L. S. Mark, R. E. Shaw, and J. B. Pittenger, “The perception of human growth,” *Scientific American*, vol. 242, no. 2, pp. 132–145, 1980.
- [17] A. Golovinskiy, W. Matusik, H. Pfister, S. Rusinkiewicz, and T. Funkhouser, “A statistical model for synthesis of detailed facial geometry,” *ACM Transactions on Graphics (TOG)*, vol. 25, no. 3, pp. 1025–1034, 2006.

- [18] Y. Tazoe, H. Gohara, A. Maejima, and S. Morishima, "Facial aging simulator considering geometry and patch-tiled texture," in *Proceedings of ACM SIGGRAPH Posters*, 2012.
- [19] J. Suo, S.-C. Zhu, S. Shan, and X. Chen, "A compositional and dynamic model for face aging," *IEEE Transactions on Pattern Analysis and Machine Intelligence (TPAMI)*, vol. 32, no. 3, pp. 385–401, 2009.
- [20] Y. Wu, N. M. Thalmann, and D. Thalmann, "A plastic-visco-elastic model for wrinkles in facial animation and skin aging," *Fundamentals of Computer Graphics*, pp. 201–213, 1994.
- [21] Y. Bando, T. Kuratate, and T. Nishita, "A simple method for modeling wrinkles on human skin," in *Proceedings of the Pacific Conference on Computer Graphics and Applications*, 2002, pp. 166–175.
- [22] B. Tiddeman, M. Burt, and D. Perrett, "Prototyping and transforming facial textures for perception research," *IEEE Computer Graphics and Applications*, vol. 21, no. 5, pp. 42–50, 2001.
- [23] I. Kemelmacher-Shlizerman, S. Suwajanakorn, and S. M. Seitz, "Illumination-aware age progression," in *Proceedings of the IEEE Conference on Computer Vision and Pattern Recognition (CVPR)*, 2014, pp. 3334–3341.
- [24] X. Shu, J. Tang, H. Lai, L. Liu, and S. Yan, "Personalized age progression with aging dictionary," in *Proceedings of the IEEE International Conference on Computer Vision (ICCV)*, 2015, pp. 3970–3978.
- [25] W. Wang, Z. Cui, Y. Yan, J. Feng, S. Yan, X. Shu, and N. Sebe, "Recurrent face aging," in *Proceedings of the IEEE Conference on Computer Vision and Pattern Recognition (CVPR)*, 2016, pp. 2378–2386.
- [26] Z. Zhang, Y. Song, and H. Qi, "Age progression/regression by conditional adversarial autoencoder," in *Proceedings of the IEEE Conference on Computer Vision and Pattern Recognition (CVPR)*, 2017, pp. 5810–5818.
- [27] G. Antipov, M. Baccouche, and J.-L. Dugelay, "Face aging with conditional generative adversarial networks," in *Proceedings of the IEEE International Conference on Image Processing (ICIP)*, 2017, pp. 2089–2093.
- [28] S. Liu, Y. Sun, D. Zhu, R. Bao, W. Wang, X. Shu, and S. Yan, "Face aging with contextual generative adversarial nets," in *Proceedings of the ACM International Conference on Multimedia (ACM MM)*, 2017, pp. 82–90.
- [29] Z. Wang, X. Tang, W. Luo, and S. Gao, "Face aging with identity-preserved conditional generative adversarial networks," in *Proceedings of the IEEE Conference on Computer Vision and Pattern Recognition (CVPR)*, 2018, pp. 7939–7947.
- [30] H. Yang, D. Huang, Y. Wang, and A. K. Jain, "Learning face age progression: A pyramid architecture of GANs," in *Proceedings of the IEEE Conference on Computer Vision and Pattern Recognition (CVPR)*, 2018, pp. 31–39.
- [31] Z. He, M. Kan, S. Shan, and X. Chen, "S2GAN: Share aging factors across ages and share aging trends among individuals," in *Proceedings of the IEEE International Conference on Computer Vision (ICCV)*, 2019, pp. 9440–9449.
- [32] X. Chen and S. Lathuilière. (2023, Sep.) Face aging via diffusion-based editing. [Online]. Available: <https://arxiv.org/abs/2309.11321>
- [33] Y. Wu, R. Wang, M. Gong, J. Cheng, Z. Yu, and D. Tao, "Adversarial uv-transformation texture estimation for 3d face aging," *IEEE Transactions on Circuits and Systems for Video Technology (TCSVT)*, vol. 32, no. 7, pp. 4338–4350, 2022.
- [34] X. Yao, G. Puy, A. Newson, Y. Gousseau, and P. Hellier, "High resolution face age editing," in *Proceedings of the International Conference on Pattern Recognition (ICPR)*, 2021, pp. 8624–8631.
- [35] J. Despois, F. Flament, and M. Perrot, "AgingMapGAN (AMGAN): High-resolution controllable face aging with spatially-aware conditional gans," in *Proceedings of the European Conference on Computer Vision (ECCV)*, 2020, pp. 613–628.
- [36] G. Zoss, P. Chandran, E. Sifakis, M. Gross, P. Gotardo, and D. Bradley, "Production-ready face re-aging for visual effects," *ACM Transactions on Graphics (TOG)*, vol. 41, no. 6, pp. 1–12, 2022.
- [37] F. Makhmudkhujav, S. Hong, and I. K. Park, "Re-aging GAN: Toward personalized face age transformation," in *Proceedings of the IEEE International Conference on Computer Vision (ICCV)*, 2021, pp. 3908–3917.
- [38] Z. He, W. Zuo, M. Kan, S. Shan, and X. Chen, "AttGAN: Facial attribute editing by only changing what you want," *IEEE Transactions on Image Processing (TIP)*, vol. 28, no. 11, pp. 5464–5478, 2019.
- [39] B. Peng, H. Fan, W. Wang, J. Dong, and S. Lyu, "A unified framework for high fidelity face swap and expression reenactment," *IEEE Transactions on Circuits and Systems for Video Technology (TCSVT)*, vol. 32, no. 6, pp. 3673–3684, 2022.
- [40] W. Li, Z. Lin, K. Zhou, L. Qi, Y. Wang, and J. Jia, "Mat: Mask-aware transformer for large hole image inpainting," in *Proceedings of the IEEE Conference on Computer Vision and Pattern Recognition (CVPR)*, 2022, pp. 10758–10768.
- [41] Y. Xu, Y. Yin, L. Jiang, Q. Wu, C. Zheng, C. C. Loy, B. Dai, and W. Wu, "Transeditor: Transformer-based dual-space gan for highly controllable facial editing," in *Proceedings of the IEEE Conference on Computer Vision and Pattern Recognition (CVPR)*, 2022, pp. 7683–7692.
- [42] H. Li, W. Wang, C. Yu, and S. Zhang, "SwapInpaint: Identity-specific face inpainting with identity swapping," *IEEE Transactions on Circuits and Systems for Video Technology (TCSVT)*, vol. 32, no. 7, pp. 4271–4281, 2022.
- [43] Y. Wang, W. Zhou, J. Bao, W. Wang, L. Li, and H. Li, "CLIP2GAN: Towards bridging text with the latent space of gans," *IEEE Transactions on Circuits and Systems for Video Technology (TCSVT)*, 2023.
- [44] F.-L. Liu, S.-Y. Chen, Y. Lai, C. Li, Y.-R. Jiang, H. Fu, and L. Gao, "DeepFaceVideoEditing: sketch-based deep editing of face videos," *ACM Transactions on Graphics (TOG)*, vol. 41, no. 4, p. 167, 2022.
- [45] T. Wei, D. Chen, W. Zhou, J. Liao, W. Zhang, G. Hua, and N. Yu, "HairCLIPv2: Unifying hair editing via proxy feature blending," in *Proceedings of the IEEE International Conference on Computer Vision (ICCV)*, 2023, pp. 23589–23599.
- [46] M. Pernuš, V. Štruc, and S. Dobrišek, "MaskFaceGAN: High resolution face editing with masked gan latent code optimization," *IEEE Transactions on Image Processing (TIP)*, vol. 32, pp. 5893–5908, 2023.
- [47] Y. Shen, C. Yang, X. Tang, and B. Zhou, "InterFaceGAN: Interpreting the disentangled face representation learned by gans," *IEEE Transactions on Pattern Analysis and Machine Intelligence (TPAMI)*, vol. 44, no. 4, pp. 2004–2018, 2022.
- [48] J. Sun, X. Wang, Y. Shi, L. Wang, J. Wang, and Y. Liu, "IDE-3D: Interactive disentangled editing for high-resolution 3d-aware portrait synthesis," *ACM Transactions on Graphics (TOG)*, vol. 41, no. 6, pp. 1–10, 2022.
- [49] J. Zhu, C. Yang, Y. Shen, Z. Shi, B. Dai, D. Zhao, and Q. Chen, "LinkGAN: Linking gan latents to pixels for controllable image synthesis," in *Proceedings of the IEEE International Conference on Computer Vision (ICCV)*, 2023, pp. 7656–7666.
- [50] Y. Liu, Q. Li, Q. Deng, and Z. Sun, "Towards spatially disentangled manipulation of face images with pre-trained StyleGANs," *IEEE Transactions on Circuits and Systems for Video Technology (TCSVT)*, vol. 33, no. 4, pp. 1725–1739, 2023.
- [51] Y. Liu, Q. Li, Q. Deng, Z. Sun, and M.-H. Yang, "GAN-based facial attribute manipulation," *IEEE Transactions on Pattern Analysis and Machine Intelligence (TPAMI)*, vol. 45, no. 12, pp. 14590–14610, 2023.
- [52] E. Perez, F. Strub, H. De Vries, V. Dumoulin, and A. Courville, "FiLM: Visual reasoning with a general conditioning layer," in *Proceedings of the AAAI Conference on Artificial Intelligence (AAAI)*, vol. 32, no. 1, 2018.
- [53] K. Karkkainen and J. Joo, "FairFace: Face attribute dataset for balanced race, gender, and age for bias measurement and mitigation," in *Proceedings of the IEEE Winter Conference on Applications of Computer Vision (WACV)*, 2021, pp. 1548–1558.
- [54] J. Johnson, A. Alahi, and L. Fei-Fei, "Perceptual losses for real-time style transfer and super-resolution," in *Proceedings of the European Conference on Computer Vision (ECCV)*, 2016, pp. 694–711.
- [55] K. Simonyan and A. Zisserman. (2015, Apr.) Very deep convolutional networks for large-scale image recognition. [Online]. Available: <https://arxiv.org/abs/1409.1556>
- [56] J. Deng, J. Guo, N. Xue, and S. Zafeiriou, "ArcFace: Additive angular margin loss for deep face recognition," in *Proceedings of the IEEE Conference on Computer Vision and Pattern Recognition (CVPR)*, 2019, pp. 4690–4699.
- [57] The FG-NET aging database. Accessed Dec. 26, 2023. [Online]. Available: [https://fipa.cs.kit.edu/433\\_451.php](https://fipa.cs.kit.edu/433_451.php)
- [58] The Face++ API for face comparing. Accessed Dec. 26, 2023. [Online]. Available: <https://www.faceplusplus.com/face-comparing/>
- [59] The FFHQ-Aging dataset. Accessed Dec. 26, 2023. [Online]. Available: <https://github.com/royorel/FFHQ-Aging-Dataset>
- [60] X. Yao, A. Newson, Y. Gousseau, and P. Hellier, "A latent transformer for disentangled face editing in images and videos," in *Proceedings of the IEEE International Conference on Computer Vision (ICCV)*, 2021, pp. 13789–13798.
- [61] Y. Alaluf, O. Tov, R. Mokady, R. Gal, and A. Bermano, "HyperStyle: StyleGAN inversion with hypernetworks for real image editing," in *Proceedings of the IEEE Conference on Computer Vision and Pattern Recognition (CVPR)*, 2022, pp. 18511–18521.

- [62] E. Richardson, Y. Alaluf, O. Patashnik, Y. Nitzan, Y. Azar, S. Shapiro, and D. Cohen-Or, "Encoding in style: a StyleGAN encoder for image-to-image translation," in *Proceedings of the IEEE Conference on Computer Vision and Pattern Recognition (CVPR)*, 2021, pp. 2287–2296.
- [63] The 81 facial landmarks shape predictor. Accessed Dec. 26, 2023. [Online]. Available: [https://github.com/codeniko/shape\\_predictor\\_81\\_face\\_landmarks](https://github.com/codeniko/shape_predictor_81_face_landmarks)
- [64] D. P. Kingma and J. Ba. (2017, Jan.) Adam: A method for stochastic optimization. [Online]. Available: <https://arxiv.org/abs/1412.6980>
- [65] Y. Choi, Y. Uh, J. Yoo, and J.-W. Ha, "StarGAN v2: Diverse image synthesis for multiple domains," in *Proceedings of the IEEE Conference on Computer Vision and Pattern Recognition*, 2020, pp. 8188–8197.
- [66] R. Liu, Y. Ge, C. L. Choi, X. Wang, and H. Li, "DivCo: Diverse conditional image synthesis via contrastive generative adversarial network," in *Proceedings of the IEEE Conference on Computer Vision and Pattern Recognition (CVPR)*, 2021, pp. 16377–16386.
- [67] R. Zhang, P. Isola, A. A. Efros, E. Shechtman, and O. Wang, "The unreasonable effectiveness of deep features as a perceptual metric," in *Proceedings of the IEEE Conference on Computer Vision and Pattern Recognition (CVPR)*, 2018, pp. 586–595.
- [68] The face detection API of baidu AI cloud. Accessed Dec. 26, 2023. [Online]. Available: <https://cloud.baidu.com/doc/FACE/s/yk37c1u4t>

TABLE VI  
STATISTICS OF AVERAGE SIMILARITY SCORES AMONG REAL FACES OF THE SAME SUBJECTS

Source age \ Target age	0-2	3-6	7-9	10-15	15-19	20-29	30-39	40-49	50-69	70+
0-2	100.00	80.24	71.55	63.75	52.81	46.45	43.44	41.54	40.68	39.69
3-6	80.24	100.00	82.83	77.64	67.68	60.77	55.68	53.01	51.85	50.23
7-9	71.55	82.83	100.00	82.64	74.80	68.43	62.73	59.69	55.90	53.37
10-14	63.75	77.64	82.64	100.00	80.86	75.00	69.87	66.75	62.61	64.37
15-19	52.81	67.68	74.80	80.86	100.00	83.32	78.97	75.68	71.57	68.10
20-29	46.45	60.77	68.43	74.99	83.32	100.00	85.39	81.90	77.38	72.31
30-39	43.44	55.68	62.73	69.87	78.97	85.39	100.00	86.76	82.22	75.40
40-49	41.53	53.01	59.69	66.75	75.68	81.90	86.76	100.00	85.69	78.62
50-69	40.68	51.85	55.90	62.61	71.57	77.38	82.22	85.69	100.00	84.17
70+	39.69	50.23	53.37	64.37	68.10	72.31	75.40	78.62	84.17	100.00

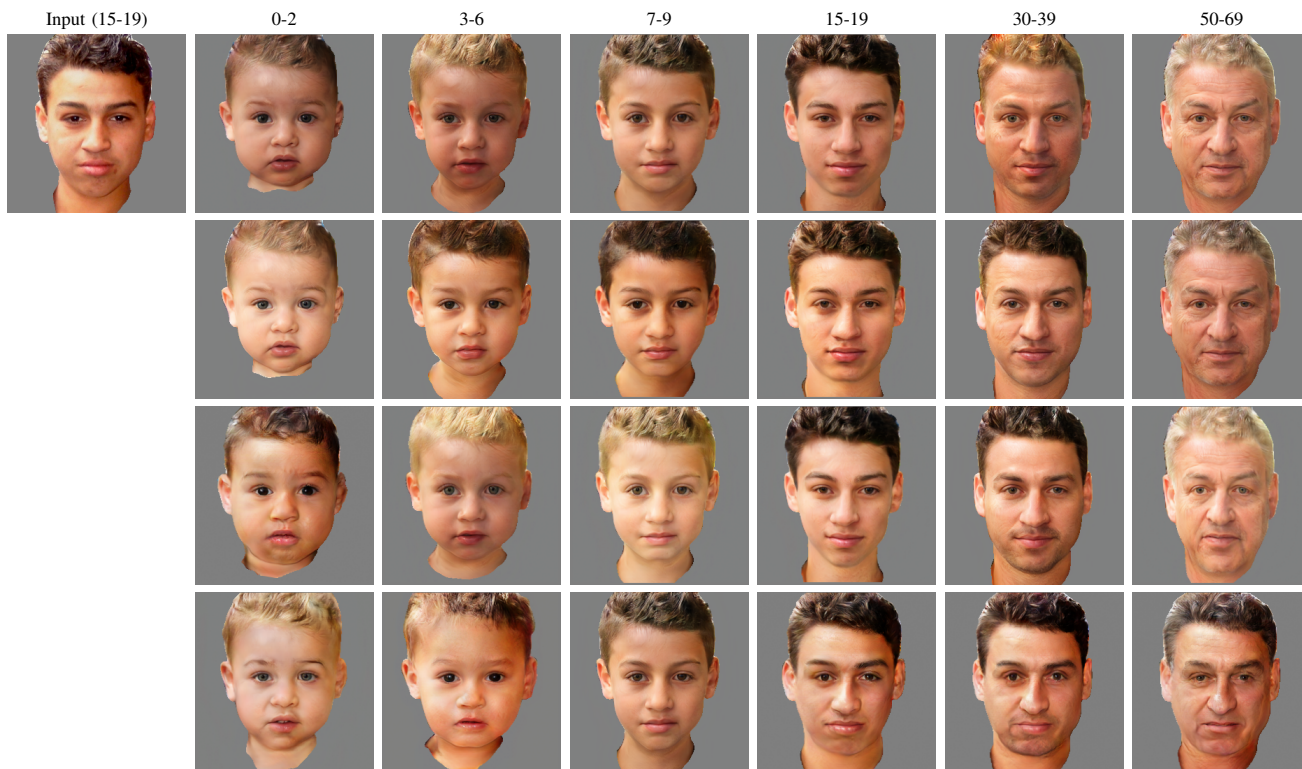


Fig. 11. Visualization of diverse age transformation results across the life cycle, generated by applying our full method to a male subject.

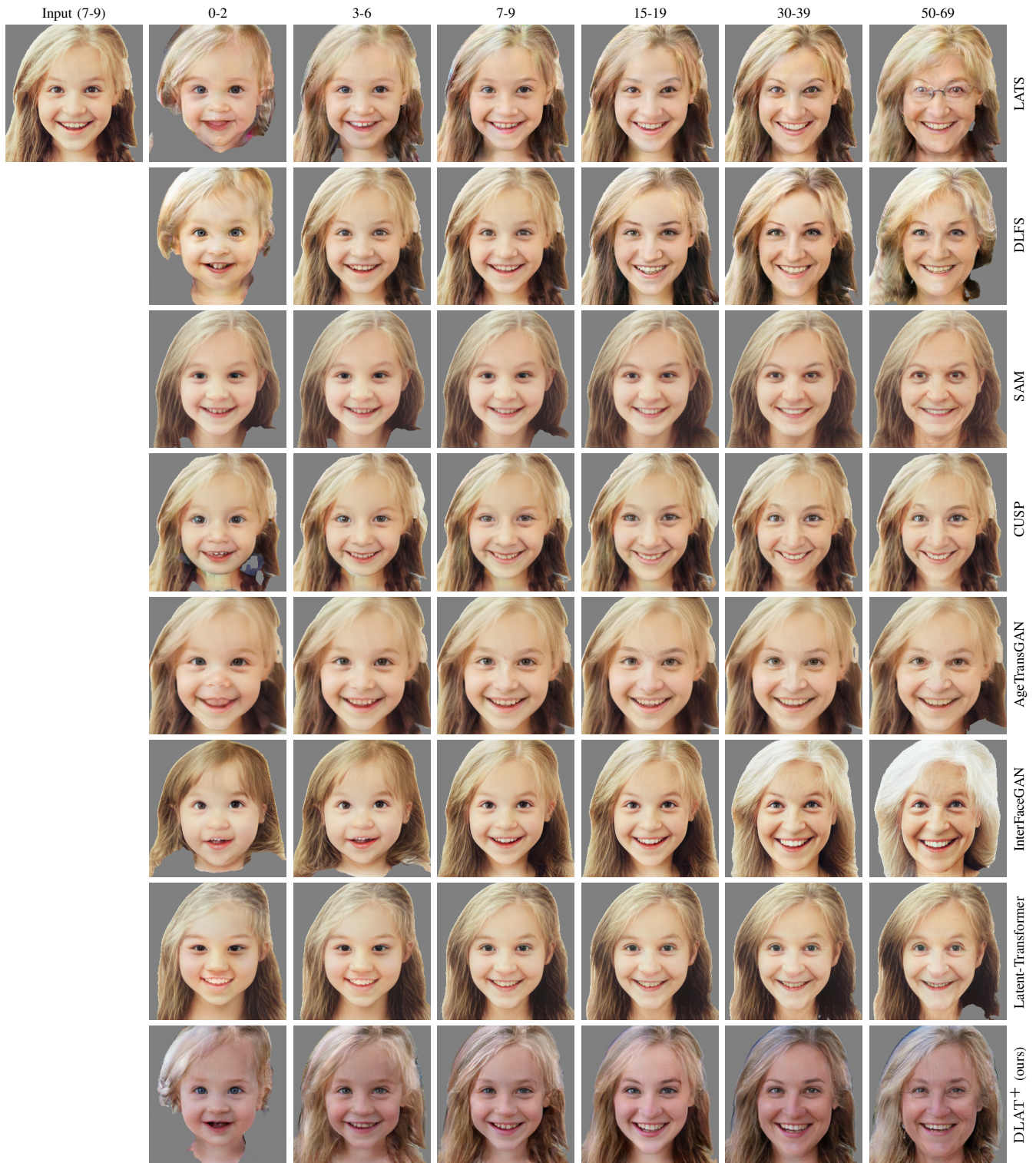


Fig. 12. Visual comparison among lifespan age transformation results of the given female subject, which are synthesized by LATS, DLFS, SAM, CUSP, AgeTransGAN, InterFaceGAN, Latent-Transformer, and our DLAT<sup>+</sup>.